

# Electronic structure and optical properties of yttrium aluminum garnet ( $\text{Y}_3\text{Al}_5\text{O}_{12}$ ) under high pressure

KE LIU<sup>a,b\*</sup>, XIAOLIN ZHOU<sup>a</sup>, JING CHANG<sup>a</sup>, JUAN CHENG<sup>a</sup>, BING DONG<sup>a</sup>

<sup>a</sup>College of Physics and Electronic Engineering, Sichuan Normal University, Chengdu 610101, P. R. China

<sup>b</sup>Institute of Atomic and Molecular Physics, Sichuan University, Chengdu 610065, P. R. China

We first introduce the latest experimental results, i.e., production of the fine nanostructured and near fully densified transparent  $\text{Y}_3\text{Al}_5\text{O}_{12}$  (YAG) bulks at high pressure and modest temperature (HPMT, 2.0-5.0 GPa & 300-500 °C). And then, We employ the first-principles plane wave pseudopotential density functional theory method in the generalized gradient approximation (GGA) to calculate the equilibrium lattice parameters, band structures, density of states, and optical properties of YAG under high pressure. The results obtained are compared with other calculations and good agreement is found.

(Received August 16, 2013; accepted March 13, 2014)

**Keywords:** High-pressure sintering, Electronic structure, Optical property, YAG

## 1. Introduction

Yttrium aluminum garnet ( $\text{Y}_3\text{Al}_5\text{O}_{12}$ ) is the most important solid-state laser host material. The properties of low-thermal expansion, high-optical transparency, low-acoustic loss, high threshold for optical damage, hardness, and general stability against chemical and mechanical changes all contribute to its success as the most widely used laser material [1-3]. Furthermore, YAG can be sintered into transparent ceramics, which makes it additionally attractive for practical applications [4-6]. Up to now, There are large number of research groups, using different methods, which have experimental and theoretically investigated the various aspects of  $\text{Y}_3\text{Al}_5\text{O}_{12}$  (YAG) and its related materials, like YAG:Nd<sup>3+</sup> and YAG:Ce<sup>3+</sup>. For instance, optical and vibrational properties of YAG crystal have been extensively studied experimentally [7-11]. The refractive index and the elastic properties of YAG have also been investigated by a variety of experimental techniques [12-15]. On the other hand, Xu et al. [16] present the results of a detailed calculation of the ground-state electronic properties of the YAG crystal, using the *ab initio* orthogonalized linear combinations of atomic orbitals (OLCAO) method within the local-density approximation (LDA). Muñoz-García et al. [17], with the periodic boundary conditions self-consistent SIESTA method, using density functional theory (DFT) within the generalized gradient approximation (GGA) as formulated by Perdew, Burke, and Ernzerhof (PBE), have made the first-principles calculations on the electronic structure and the atomistic structure of YAG up to 40 GPa with no indication of any phase change. We have investigated the thermodynamic properties of YAG under pressure up to 50GPa, as reported

by us earlier [18]. But, to the best of our knowledge, there are lack of theoretical investigations on electronic structure and optical properties of YAG crystal under high pressure because of its enormously complicated crystal structure which renders detailed *ab initio* quantum-mechanical calculation computationally too demanding. It is known that YAG has a *bcc* structure (space group  $\text{Ia}\bar{3}d$  or  $O_h^{10}$ ) with 160 (80) atoms in the cubic (primitive) cell. The Y ions occupy the 24(c) sites and each are dodecahedroally coordinated to eight O. The O atoms occupy the 96(h) sites. There are two different sites for Al, Al<sub>oct</sub> occupy the 16(a) site with an octahedral point symmetry ( $C_{3i}$ ) and Al<sub>tet</sub> occupy the 24(d) sites with a tetrahedral point symmetry ( $S_4$ ). The garnet structure can be viewed as interconnected octahedraons, tetrahedrons, and dodecahedrons with shared O atoms at the corners [16]. In the present study, the structural, electronic, and optical properties of YAG crystal under high pressure were studied based on the density function theory calculations.

## 2. Experimental procedure

We used the lab-synthesized YAG powder, by alcohol-water co-precipitation method [19], as starting material. The powder is checked by x-ray diffraction (XRD). As shown in Fig. 1, the starting powder shows a pure phase of YAG and high crystalline quality. The average size of crystallites is estimated to be about 30 nm from Scherer's formula [20]. High-pressure sintering experiments were carried out using a 6 × 800 MN large-volume cubic-type multi-anvil high-pressure apparatus [21]. As shown in Fig. 2, the as-prepared transparent nano-ceramic has been prepared using high

pressure and modest temperature (HPMT) sintering technique at 5 GPa and heating for 30 min at 450 °C, which has been described in detail elsewhere [22]. The relative density reaches 99.68 % ( $\rho_{\text{theo}} = 4.56 \text{ g/cm}^3$ ). With the traditional method of free pressure sintering to obtain the  $\text{Y}_3\text{Al}_5\text{O}_{12}$  ceramics having such a density is possible only at temperatures above 1700 °C [23].

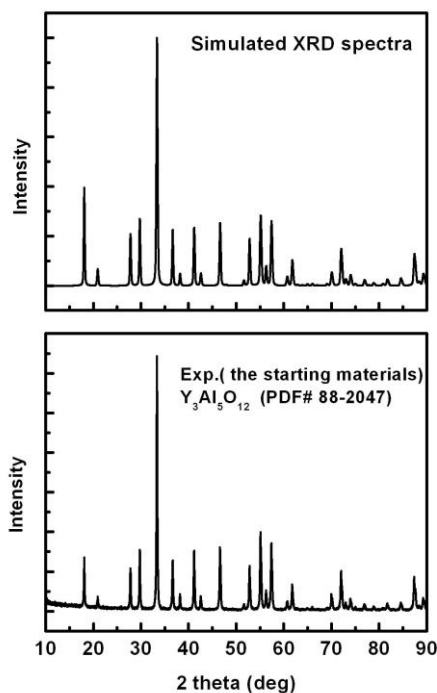


Fig. 1. Simulated XRD spectra of YAG in comparison with the measured experimental XRD spectrum of the starting material is synthesized by alcohol-water co-precipitation method, with a uniform phase composition of YAG.

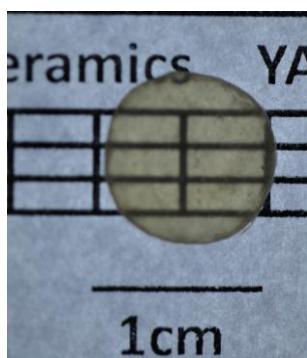


Fig. 2. The image of as-prepared YAG nanoceramic sample. The sample sintered at 5.0 GPa/450 °C for 30 min is highly transparent and shows no apparent cracks.

### 3. Models and methods

In this work, all first-principles calculations were performed with the CASTEP code [24]. The ultrasoft pseudopotential [25] was employed to describe the interaction between ions and electrons. Both the Perdew–Wang 1991 (PW91) [26] generalized gradient approximation (GGA) [27] and the local-density approximation (LDA) [28] were used to describe the exchange and correlation potentials. Wave functions of valence electronics expand in the form of plane wave basis sets. Pseudo atomic calculations are performed for Y ( $4d^1 5s^2$ ), Al ( $3s^2 3p^1$ ) and O ( $2s^2 2p^4$ ). A kinetic cut-off of plane wave 380eV and a  $3 \times 3 \times 3$  Monkhorst–Pack [29] grid for Brillouin zone sampling are used throughout. The threshold of  $10^{-7}$  eV/atom is used to determine whether the self-consistent progress has been converged.

### 4. Results and discussion

#### 4.1. Structural analysis

To assure the correct description of the structure, a simulation of the XRD diffraction pattern was run using the Reflex module of Materials Studio software. Fig. 1 shows the comparison between the experimental XRD pattern and the simulated pattern of YAG configuration having the same grain size (30 nm) at the same wavelength ( $1.540562 \text{ \AA}$ ) as those used in previous experiment. The correspondence of the simulated XRD pattern in this work with the experimental XRD spectrum gives us confidence to investigate the structure and optical properties of YAG at high pressure.

It is well known that LDA usually underestimates the lattice constants and overestimates the elastic constants, while GGA overestimates the lattice constants and underestimates the elastic constants [30, 31]. For this reason, both the LDA and GGA methods were used to obtain the lattice parameters and bulk modulus.

We take a series of lattice constants  $a$  to obtain the total energy  $E$  and the corresponding primitive cell volume  $V$ . The calculated equilibrium lattice constants  $a$ , zero-pressure bulk modulus  $B_0$  and its pressure derivation  $B'_0$  from the Natural strain third-order EOS [32] are listed in Table 1, together with our experimental data  $12.004 \text{ \AA}$  by x-ray diffraction (XRD) and other theoretical results. The agreement among them is good.

Table 1. Our GGA- and LDA-calculated lattice constants (in Å), bulk moduli (in GPa), pressure derivative of bulk modulus, compared with experimental and other calculated results.

	Present calc.		Other calc.	Expt.
$a$	12.337 (GGA)	11.827 (LDA)	11.904 <sup>a</sup> , 12.114/11.691 <sup>b</sup>	12.004 (present) 12.000 <sup>c</sup> , 12.0089 <sup>d</sup> , 12.0425/12.0545 <sup>e</sup>
$B_0$	207.7 (GGA)	209.2 (LDA)	228.6/220.7/221.1 <sup>f</sup> /221.0 <sup>g</sup>	220.0 <sup>h</sup> , 185.2 <sup>i</sup> , 189.0 <sup>j</sup>
$B'_0$	3.80 (GGA)	3.94 (LDA)	4.60/4.12/4.00 <sup>k</sup> , 3.09 <sup>m</sup>	4.42 <sup>n</sup>

<sup>a</sup>From the OLCAO-LDA method [16].

<sup>b</sup>From the PBE / LDA method [17].

<sup>c</sup>Ref. [33].

<sup>d</sup>Ref. [34].

<sup>e</sup>samples prepared at 2 and 6 GPa [35].

<sup>f</sup>From the Fourth order polynomial/ Murnaghan EOS/ Birch-Murnaghan EOS [16].

<sup>g</sup>From the PBE [17].

<sup>h</sup>Ref. [13].

<sup>i</sup>Ref. [14]

<sup>j</sup>Ref. [15]

<sup>k</sup>From the Fourth order polynomial/ Murnaghan EOS/ Birch-Murnaghan EOS [16].

<sup>m</sup>From the PBE [17]

<sup>n</sup>Ref. [36]

Using the quasi-harmonic Debye model [37], in Fig. 3, we illustrate the calculated  $V/V_0$  ( $V_0$  is the zero-pressure equilibrium primitive cell volume) dependences on pressure  $P$ . Our calculated EOS agrees well with other theoretical results [17]. By fitting these GGA data to second-order polynomials of the applied pressure, we obtained the following relationship at  $T=0$  K.

$$V/V_0 = 0.99893 - 0.0046P + 2.8259 \times 10^{-5} P^2 \quad (1)$$

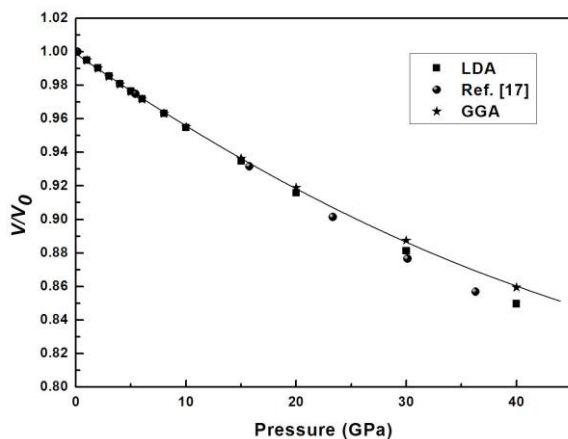


Fig. 3. The normalized volume  $V/V_0$  of YAG as a function of pressure  $P$ , compared with other theoretical results [17].  $V_0$  is the zero pressure equilibrium volume at 0K.

## 4.2 Electronic structure

The GGA-calculated band structure of YAG crystal at 0GPa, 20GPa and 40GPa are displayed in Fig. 4. It is observed that the top of valence band (VB) and the bottom of conduction band (CB) are both exactly located at highly symmetric  $\Gamma$  point. Thus, a direct band gap is formed and the value is about 4.15 eV, (4.45 eV for LDA), which is smaller than the optical experimental value of 6.4 eV [8]. Such an underestimation of the gap value is typical of the GGA and LDA calculations. Further, it can be seen from the graph, in addition to changes in the band gap, there is no difference in appearance of these three cases. Muñoz-García et al. [17] found that the CB edge was made of a simple band, of a main Y (4d +5s) character. However, we note that the CB edge at  $\Gamma$  in YAG consists of two rather well-separated bands, which is consistent with Xu et al. [16]. This could be due to the presence of two nonequivalent cations in YAG and the specific symmetry of the crystal.

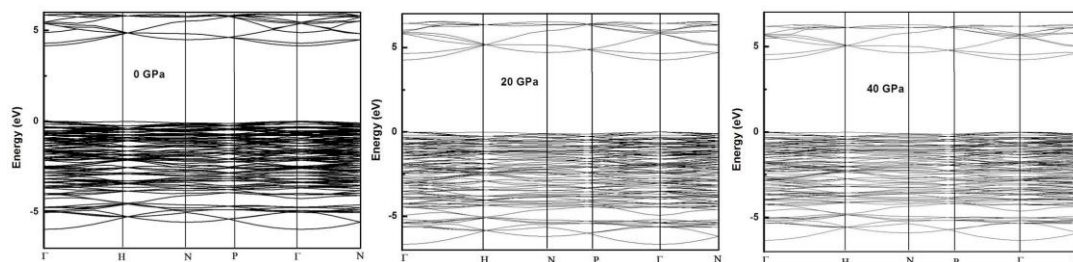


Fig. 4. The calculated band structure of YAG at 0GPa, 20GPa and 40GPa.

The variations of the GGA-band gap as a function of pressure are illustrated in Fig. 5. It is shown that, at a lower pressure, the band gap is sensitive to pressure and increases drastically with increasing pressure. However, when the pressure is above 20 GPa, the band gap just has a moderate increase. We are not aware of any experimental measurements related to the change of gap under pressure.

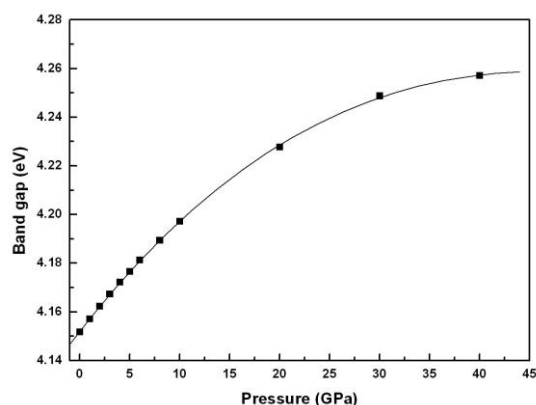


Fig. 5. Calculated band gap as functions of the pressure.

To have a better understanding of different contributions of Y, Al and O, we illustrate the total DOS and the projected local density of states (PDOS) onto different atoms in Fig. 6. The DOS spectra in Fig. 6 indicate that CB originates mainly from the contribution of 4d orbital of Y. The major contribution to the VB from -18.31 to -14.70 eV is from the O 2s orbital. The VB from -6.89 eV to the top of valence band comes mainly from the O 2p orbital, with minor contribution by Y 4d, 5s and Al 3s, 3p orbitals.

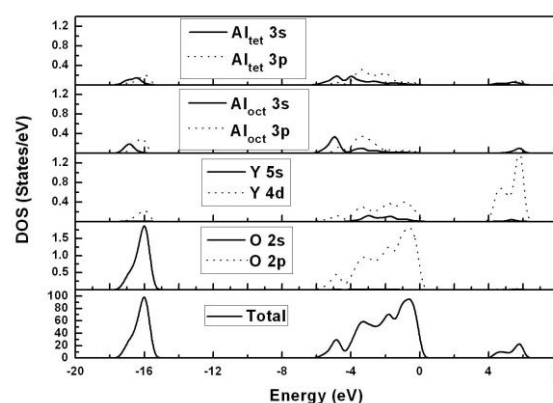


Fig. 6. The calculated total density of states (DOS) and its projected local density of states (PDOS) of YAG.

### 4.3 Optical properties

We now carry out the theoretical study on the optical properties of this material. It is well known that the dielectric function is a very important parameter for a material because it is the fundamental feature of the linear response to an electromagnetic wave and uniquely determines the propagation behavior of the radiation within. All other optical constants, such as the absorption coefficient, reflectivity spectra, and the electron energy-loss spectra could be deduced from the imaginary part  $\epsilon_2(\omega)$  and the real part  $\epsilon_1(\omega)$  of the dielectric function. The imaginary part  $\epsilon_2(\omega)$ , can be given by calculating the momentum matrix elements between the occupied and unoccupied wave functions using selection rules, and the real part  $\epsilon_1(\omega)$ , can be derived from  $\epsilon_2(\omega)$  using the Kramer–Kronig relationship [38, 39].

The calculated dielectric functions of YAG are displayed in Fig. 7 in a range of energy, 0–18 eV. Below about 4 eV (the band-gap region),  $\epsilon_2(\omega)$  is zero and  $\epsilon_1(\omega)$  tends to be a constant as the photon energy approaches zero, the calculated static dielectric constant  $\epsilon_1(0)$  was 1.43. It is an advantageous attempt of theoretical studies to identify the transitions that are responsible for the peaks in  $\epsilon_2(\omega)$  using the calculated band structures. The major peak located around 6 eV is attributed to the interband transitions from O 2p valence

band to Y 4d conduction band. This peak is very strong and very much far higher than other peaks. On the other hand, it is shown in Fig. 7 that, as pressure increases from 0 to 40 GPa, there is a blue-shift. In addition, the magnitude of the peaks decreases.

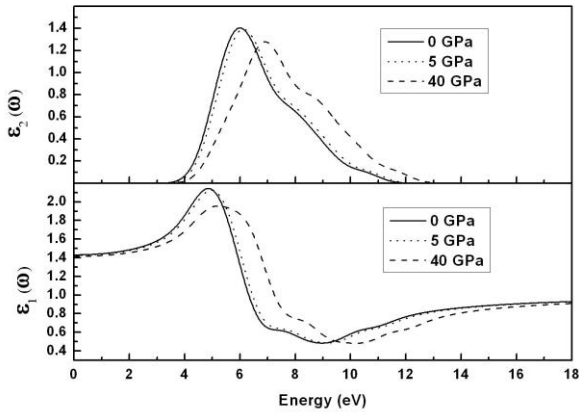


Fig. 7. The calculated imaginary part  $\epsilon_2(\omega)$  and real part  $\epsilon_1(\omega)$  of the dielectric function of the ferroelectric YAG crystal as a function of the photon energy.

The refractive index provides useful information about the optical properties of the material. The extinction coefficient directly describes the attenuation of electromagnetic waves within the material and is also known as a damping constant or attenuation coefficient. The refractive index and the extinction coefficient are given in Fig. 8. The static refractive index  $n(0)$  is found to have a value of 1.2. This value increases with increasing the energy in the transparency region and reaches a peak at about 4.98 eV. It then decreases to a minimum at 9.3 eV. The local maxima of the extinction coefficient  $k(\omega)$  corresponds to the zero of  $\epsilon_1(\omega)$ . The origin of the structures in the imaginary part of the dielectric function also explains the structures in the refractive index.

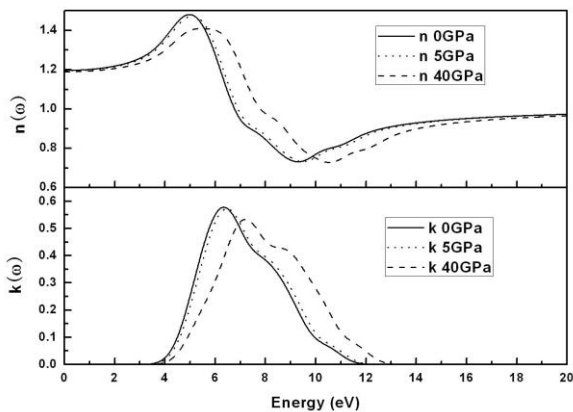


Fig. 8. Calculated refractive index  $n(\omega)$  and extinction coefficient  $k(\omega)$  of YAG.

Other optical constant can be also calculated from the complex dielectric function. Fig. 9 (a)–9(c) display the calculated optical constants of YAG on photon energy dependence of absorption spectrum  $\alpha(\omega)$ , energy-loss spectrum, and reflectivity, respectively. These parameters are very important to the optical material and related applications [40].

As shown in Fig. 9(a), the absorption edge starts from about 4 eV, corresponding to the energy gap. According to our dielectric function calculation, the energy of each absorption peak is due to the transition of electron excitation from the VB to the CB in the electronic energy band structure. The first peak in the absorption spectrum is at 6.54 eV. This originates from a transition from the O 2p electron states located at the top of the valence bands to the empty Y 4d electron states dominating the bottom of the conduction bands. The electron energy loss function  $L(\omega)$  is an important factor describing the energy loss of a fast electron traversing in a material. Prominent peaks in  $L(\omega)$  spectra represent the characteristics associated with the plasma oscillations and the corresponding frequencies are the so-called bulk plasma frequency  $\omega(p)$ , which occurs where  $\epsilon_2 < 1$  and  $\epsilon_1$  reaches the zero point [41]. The main peak of  $L(\omega)$  (Fig. 9b) is at about 8.80 eV. The variation of reflectance as a function of photon energy is displayed in Fig. 9(c). The dynamic reflectance corresponds to the ratio of the intensities of the incident and reflected electric fields. In the low energy regime ( $\leq 2$  eV) and above 12 eV, the reflectance curves are nearly flat with reflectivity values between about 0.008 to 0.009 eV. Furthermore, this value increases with increasing the energy and reaches a peak of 0.072 at about 6.37 eV. The small value of reflectance ensures its applications as transparent ceramics. The reflectance presented in this study could serve as a reference for future experimental studies on YAG.

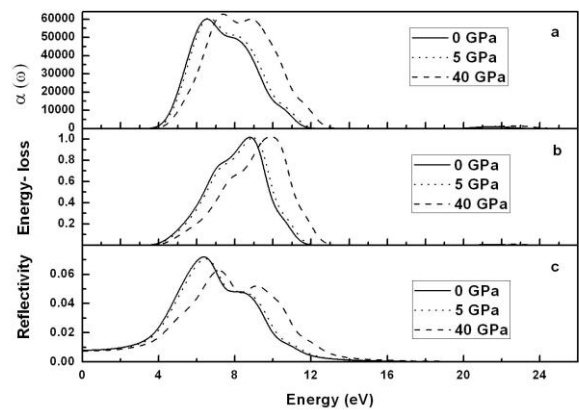


Fig. 9. Calculated absorption spectra, energy-loss spectrum and reflectivity spectra of YAG.

In summary, the structural, electronic and optical

properties of YAG under pressure were studied in detail. Calculations show that there is a typical underestimate (overestimates) of lattice parameters in the LDA (GGA) approximation. A direct band gap is formed and the value is about 4.15 eV (for GGA) and 4.45 eV (for LDA) at highly symmetric  $\Gamma$  point. The dielectric function, refractive index, extinction coefficient, absorption spectrum, energy loss coefficient and reflectivity are also successfully obtained. Using the band structure, the interband contribution to optical response functions was analyzed. Our studies may serve as a reference for YAG in the application of optoelectronics.

### Acknowledgements

This work is supported by the China 973 Program (Grant No. 2011CB808205) and the National Natural Science Foundation of China (Grant No. 11027405, 11304211) and the Scientific Reserch Fund of SiChuan Provincial Education Department (Grant No. 12ZBL104, 11ZB079, 09ZDL01).

### References

- [1] R. C. Powell, *Physics of Solid State Laser Materials*, AIP, New York, (1998).
- [2] R. Qindeel, N. Bidin, R. Zia, Y. M. Daud, *Optoelectron. Adv. Mater.- Rapid Comm.* **5**, 331 (2011).
- [3] V. Kokenyesi, I. Popovich, M. Sichka, A. Kikinshi, L. Daroczi, D. Beke, Y. Sharkany, C. S. Hegedus, *Optoelectron. Adv. Mater.- Rapid Comm.* **1**, 171 (2007).
- [4] Y. Rabinovitch, D. Tétard, M. D. Faucher, M. Pham-Thi, *Optical Materials* **24**, 345 (2003).
- [5] N. Saito, S. I. Matsuda, T. Ikegami, *Journal of the American Ceramic Society* **81**, 2023 (1998).
- [6] E. Zych, D. Hreniak, W. Stręk, L. Kępiński, *Journal of Alloys and Compounds* **341(1-2)**, 391 (2002).
- [7] J. P. Hurrell, S. P. S. Porto, I. F. Chang, S. S. Mitra, R. P. Bauman, *Phys. Rev.* **173**, 851 (1968).
- [8] G. A. Slack, D. W. Oliver, R. M. Chrenko, S. Roberts, *Phys. Rev.* **177**, 1308 (1969).
- [9] Y. Zhan, P. D. Coleman, *Appl. Opt.* **23**, 548 (1984).
- [10] T. Tomiki, F. Fukudome, M. Kaminao, M. Fujisawa, Y. Tanahara, T. Futemma, *J. Phys. Soc. Jpn.* **54**, 4429 (1988); **58**, 1801 (1989).
- [11] T. Tomiki, Y. Ganaha, T. Shikenbrau, T. Futemma, M. Yuri, Y. Aiura, H. Fukutani, H. Kato, J. Tamashiro, T. Miyahara, A. Yonesu, *J. Phys. Soc. Jpn.* **62**, 1388 (1993); **65**, 1106 (1996).
- [12] R. D. Shannon, M.A. Subramanian, T. H. Allik, H. Kimura, M. R. Kokta, M. H. Randies, G. R. Rossman, *J. Appl. Phys.* **67**, 3798 (1990).
- [13] A. M. Hofmeiser, K. R. Campbell, *J. Appl. Phys.* **72**, 638 (1992).
- [14] P. R. Stoddart, P. E. Ngoepe, P. M. Mjwara, J. D. Comins, G. A. Saunders, *J. Appl. Phys.* **73**, 7298 (1993).
- [15] W. J. Alton, A. J. Barow, *J. Appl. Phys.* **32**, 1172 (1967).
- [16] Y. N. Xu, W. Y. Ching, *Phys. Rev. B* **59**, 10530 (1999).
- [17] A. B. Muñoz-García<sup>1</sup>, E. Anglada, L. Seijo, *International Journal of Quantum Chemistry* **109**, 1991 (2009).
- [18] K. Liu, D. W. He, X. L. Zhou, *J. Therm. Anal. Calorim.* **111**, 289 (2013).
- [19] S. H. Tong, T. C. Lu, and W. Guo, *Materials Letters* **61**, 4287 (2007).
- [20] P. Scherrer, N. G. W. Gottingen, *Math-Pys.* **Kl. 2**, 96 (1918).
- [21] C. Chen, D. He, Z. Kou, F. Peng, L. Yao, R. Yu, Y. Bi, *Adv. Mater.* **19**, 4288 (2007).
- [22] K. Liu, D. W. He, H. M. Wang, T. C. Lu, F. Li, X. L. Zhou, *Scripta Materialia.* **66**, 319 (2012).
- [23] J. G. Li., T. Ikegami, J. H. Lee, T. Mori, *J. Am. Ceram. Soc.* **83**, 961 (2000).
- [24] M. D. Segall, P. L. D. Linda, M. J. Probert, C. J. Pickard, P. J. Hasnip, S. J. Clark, M. C. Payne, *J. Phys.: Condens. Matter* **14**, 2717 (2002).
- [25] D. Vanderbilt, *Phys. Rev. B* **41**, 7892 (1990).
- [26] J. P. Perdew, Y. Wang, *Phys. Rev. B* **45**, 13244 (1992).
- [27] J. P. Perdew, K. Burke, M. Ernzerhof, *Phys. Rev. Lett.* **77**, 3865 (1996).
- [28] D. M. Ceperley, B. J. Alder, *Phys. Rev. Lett.* **45**, 566 (1980).
- [29] J. Monkhorst, J. D. Pack, *Phys. Rev. B* **13**, 5188 (1976).
- [30] R. Yu, X. F. Zhang, *Appl. Phys. Lett.* **86**, 121913 (2005).
- [31] C. Stampfl, W. Mannstadt, R. Asahi, A. J. Freeman, *Phys. Rev. B* **63**, 155106 (2001).
- [32] J. P. Poirier, A. Tarantol, *Phys, Earth Planet Int.* **109**, 1 (1998).
- [33] F. Euler, J. A. Bruce, *Acta Crystallogr* **19**, 971 (1965).
- [34] R. P. Yavetskiy, E. A. Vovk, A. G. Doroshenko, M. I. Danylenko, A. V. Lopin, I. A. Petrusha, V. F. Tkachenko, A. V. Tolmachev, V. Z. Turkevich, *Ceramics International* **37**, 2477 (2011).
- [35] A. Lukowiak, R. J. Wiglusz, M. Maczka, P. Gluchowski, W. Strek, *Chemical Physics Letters* **494**, 279 (2010).
- [36] Y. K. Yogurtcu, A. J. Miller, G. A. Saunders, *J. Phys. C* **13**, 6585 (1980).
- [37] M. A. Blanco, E. Francisco, V. Luana, *Comp. Phys. Commun.* **158**, 57 (2004).
- [38] S. Saha, T. P. Sinha, *Phys. Rev. B* **62**, 8828 (2000).
- [39] M. Q. Cai, Z. Yin, M. S. Zhang, *Appl. Phys. Lett.* **83**, 2805 (2003).
- [40] X. D. Zhang, M. L. Guo, W. X. Li, C. L. Liu, *J. Appl. Phys.* **103**, 063721 (2008).
- [41] J. S. De Almeida, R. Ahuja, *Phys. Rev. B* **73**, 165102 (2006).

\*Corresponding authors: lkworld@126.com;  
Zhouxl\_wuli@163.com